Passive Aerodynamic Drag Balancing in a Flapping-Wing Robotic Insect

P. S. Sreetharan[1]
e-mail: pratheev@post.harvard.edu

R. J. Wood

School of Engineering and Applied Science,
Harvard University,
60 Oxford Street,
Cambridge, MA 02138-1903

Flapping-wing robotic platforms based on Dipteran insects have demonstrated lift to weight ratios greater than 1, but research into regulating the aerodynamic forces produced by their wings has largely focused on active wing trajectory control. In an alternate approach, a flapping-wing drivetrain design that passively balances aerodynamic drag torques is presented. A discussion of the dynamic properties of this millimeter-scale underactuated planar linkage accompanies an experimental test of an at-scale device. This mechanism introduces a novel strategy for regulating forces and torques from flapping wings, using passive mechanical elements to potentially simplify control systems for mass and power limited flapping-wing robotic platforms. [DOI: 10.1115/1.4001379]

Keywords: linkages, robotic systems, robot kinematics, bio-inspired robotics, power transmission

1 Introduction

Biological insects are among nature's most nimble fliers, but the kinematic and aerodynamic mechanisms that enable their flight remain an active area of research. Much progress has been made in understanding the biological form and function of flight-capable insects as well as the aerodynamic properties of flapping-wing flight [1–3].

Recent developments in millimeter-scale fabrication processes have led to rapid progress toward creating microrobotic insects based on their biological counterparts [4–6]. Insects of the order Diptera have inspired several projects to create similarly scaled micro-air vehicles (MAVs), including Berkeley's micromechanical flying insect (MFI) and the Harvard microrobotic fly (HMF) [7,8].

Generating aerodynamic forces of a sufficient magnitude is a primary concern for both biological and microrobotic fliers, but hovering and executing flight maneuvers also require subtle control over these forces. While the HMF design has recently demonstrated the generation of sufficient lift to support the mass of its aeromechanical structure (see Ref. [8]), additional mechanisms allowing control over the aerodynamic forces produced by the wings are necessary in order to achieve stable flight.

The addition of kinematic control inputs has been demonstrated to enable active control over the stroke amplitude of each wing of an at-scale microrobotic insect, though not yet on a flight worthy platform [9]. Evidence exists that biological organisms similarly use flight control muscles to actively apply kinematic perturbations to their wing trajectories, though the complete behavior of these muscles in Dipteran insects is not yet fully understood [2,10].

This article describes a drivetrain applicable to airborne microrobotic platforms scaled similarly to Dipteran insects. Unique among such robotic devices, this drivetrain exhibits passive aeromechanical regulation of imbalanced torques (PARITy) and will be referred to as the PARITy drivetrain, or simply the PARITy. Existing flapping-wing MAV platforms including the MFI, the HMF, and others (see University of Tokyo's butterfly type ornithopter [11], Microbat [12], Delfly from the Delft University of Technology, and MAVs from the University of Delaware [13]) enforce a kinematic relationship between power actuation strokes and wingstroke angles. In contrast, wingstroke angles produced by the PARITy drivetrain are underconstrained. An underconstrained wing configuration is not in itself an original concept: The HMF incorporates underconstrained wing angles of attack to enable the generation of lift [8].

However, the PARITy drivetrain design introduces a novel paradigm for controlling the aerodynamic forces created by flapping wings. In contrast with designs that produce deterministic kinematic relationships between actuation strokes and wingstroke angles, the PARITy design creates deterministic relationships between the *aerodynamic forces* experienced by each wing. This behavior is realized by introducing additional degrees of freedom to the system, causing the relationship between wing trajectory and actuation stroke to be kinematically underconstrained. During operation of the PARITy, tuned system dynamics passively alter wing trajectories in a manner that enforces the desired relationships between aerodynamic forces at each wing. Under this paradigm, flight control strategies would focus on changing system dynamics to alter the enforced force relationships. It is hoped that incorporating mechanical features that dynamically respond to aerodynamic forces will alleviate requirements on flight control systems for mass and power limited aeromechanical platforms.

The PARITy drivetrain delivers power from a single actuator to two wings in a manner that balances the aerodynamic drag torques created at each wing. Its design is inspired by the automobile differential, and many parallels between the two mechanisms will be noted. This article will first discuss the contrasting power distribution strategies of the displacement-balancing HMF drivetrain and the torque-balancing PARITy, followed by a description of the PARITy drivetrain's kinematic design. The PARITy drivetrain's dynamic behavior, especially those features responsible for balancing aerodynamic drag torques, will then be treated in a simplified theoretical analysis supported by numerical simulations. Finally, the simulated performance will be corroborated by experimental results from a PARITy drivetrain manufactured in the laboratory.

2 A Displacement-Balancing Drivetrain

The drivetrain for a flapping-wing MAV shares many characteristics with that of a classic two-wheel-drive automobile. Both devices must deliver power from a single actuator to two end-

[1]Corresponding author.

Contributed by the Mechanisms and Robotics Committee of ASME for publication in the JOURNAL OF MECHANICAL DESIGN. Manuscript received August 19, 2009; final manuscript received February 2, 2010; published online May 3, 2010. Assoc. Editor: James Schmiedeler.

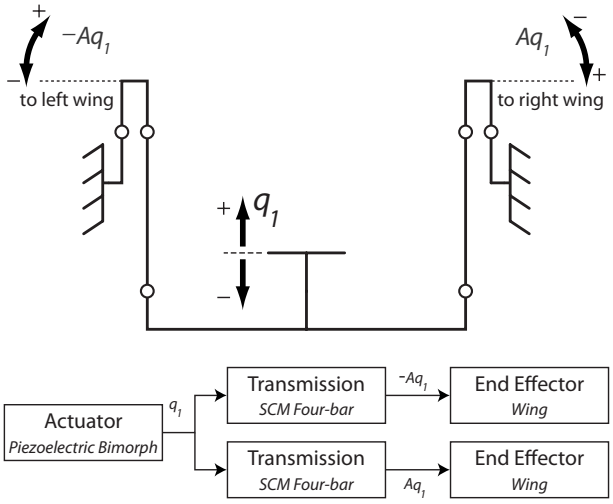

Fig. 1 Kinematic diagram and representative block diagram for the simple HMF transmission

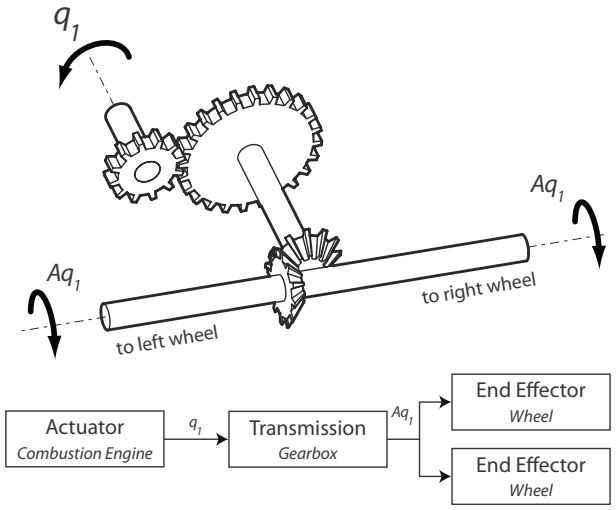

Fig. 2 A simplified automobile drivetrain, analogous to the HMF transmission

effectors. In the case of an automobile, the actuator is an internal combustion engine whose single output shaft must drive two wheels. In the HMF, an archetypal flapping-wing MAV, the actuator is a piezoelectric bimorph that must deliver power to two wings [8].

In these devices, the drivetrain, defined here as a mechanism connecting the actuator to the two end-effectors, must accomplish two tasks: It must map the actuation stroke to the end-effector strokes and it must distribute the available power among the two end-effectors. The first task is accomplished by a device called a transmission. The automobile traditionally uses a 1DOF gearbox, though several discrete transmission ratios can be automatically or manually selectable. The HMF transmission is a 1DOF flexure-based four-bar linkage.

A mechanistically simple method for executing the second task, the apportionment of available power, is to constrain the relationship of end-effector displacements. This is the strategy used in the HMF; its drivetrain, shown in Fig. 1, flaps both wings on symmetric trajectories. An analogous drivetrain for an automobile that produces balanced wheel trajectories is also presented.

Balanced displacement of each end-effector, however, is often not the ideal apportionment of actuator power. For example, the automobile drivetrain from Fig. 2 is not used in practice because of its poor performance during turns. Executing a turn without a wheel slip requires the inner and outer wheels to rotate at different speeds. A drivetrain that distributes power in this equal-displacement fashion will waste power by causing one or both wheels to slip during a turn.

In a flapping-wing MAV, apportioning power so as to execute symmetric wing trajectories is also not an ideal case. Hovering in still air does not require balancing the *trajectory* of each wing; rather, it requires balancing the *aerodynamic reaction forces* from each wing. With the eventual design intent of controlling the orientation and velocity of a MAV in free flight, the wing trajectories are interesting only as an instrument to create the desired aerodynamic forces. Researchers are currently attacking the problem of balancing and controlling aerodynamic forces on the wings by introducing fully determined kinematic perturbations to wing-stroke angles (see Ref. [9]) or both stroke and attack angles (see Ref. [7]), with the vision that a control system will calculate appropriate wing trajectories.

An alternative approach, however, is to create a mechanical drivetrain that operates directly on aerodynamic forces and torques. The kinematics of such a drivetrain must be capable of producing complex relative wing motions. The drivetrain must also respond correctly to asymmetric aerodynamic conditions presented to each wing, passively altering wing trajectories to produce the desired aerodynamic force and torque relationships without active control.

The PARITy drivetrain is a first incarnation of this alternative approach and, in contrast with the displacement-balancing HMF drivetrain, passively apportions actuator power so as to balance the aerodynamic drag torques realized at each wing, allowing wingstroke angles to decouple accordingly. This behavior is enabled by the introduction of a passive load-balancing element that exploits system dynamics to balance load torques on the two wings.

3 The Parity Drivetrain

3.1 A Torque-Balancing Drivetrain. The concept of a drivetrain that balances load torques is not a new one: A mechanism is ubiquitous in automotive design, which, in its simplest form, delivers a balanced torque to two output shafts, allowing their rotations to decouple. This load-balancing element, known as a differential, functions by introducing an additional degree of freedom to the 1DOF drivetrain of Fig. 2. In an automobile drivetrain incorporating a differential, the engine shaft rotation q_1 no longer determines the individual wheel rotations, rather, it prescribes the *sum* of the wheel rotations. The degree of freedom q_2 introduced by the differential is proportional to the *difference* of the wheel rotations and has no associated actuator. The differential mechanism, shown schematically in Fig. 4, is designed such that q_2 passively follows a trajectory that results in an equal torque on each of the two output shafts. The individual wheels are allowed to follow complex trajectories, but power from the engine will be distributed so as to balance the output torques.

The PARITy drivetrain, which functions as both a transmission and a load-balancing element in the context of a flapping-wing MAV, is presented in Fig. 3. Though both the PARITy and an automobile drivetrain deliver power from an actuation stroke q_1 to two output end-effectors, the kinematic design of the PARITy departs from that of an automobile drivetrain in several ways:

1. The PARITy input and outputs are reciprocating motions. In an automobile drivetrain, the input and outputs are continuous rotations.
2. The actuation stroke q_1 applied to the PARITy input prescribes the difference of output wing angles while their sum is undetermined. In an automobile, the sum of the output wheel rotations is prescribed while their difference is undetermined.

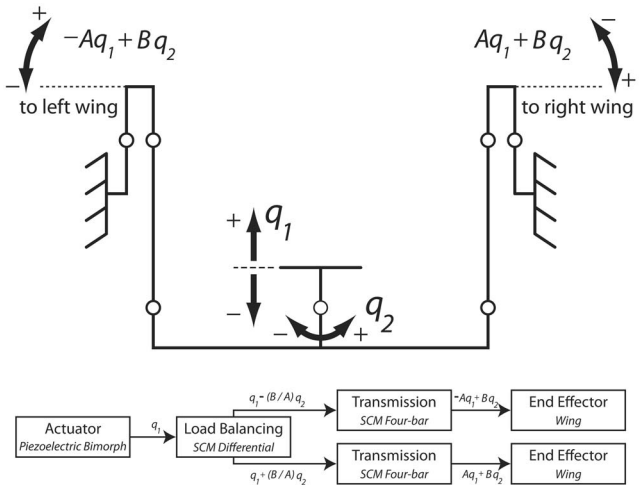

Fig. 3 Kinematic diagram and representative block diagram for the PARITy drivetrain

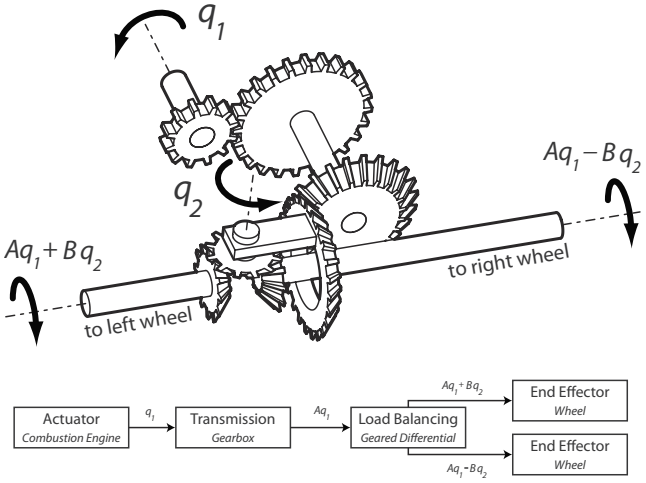

Fig. 4 A classic automobile drivetrain, analogous to the PARITy design, incorporating a transmission and a differential

3. An automobile uses a single transmission upstream of the load-balancing differential, while the PARITy is characterized by dual transmissions downstream of the load-balancing element (Figs. 3 and 4).

Of these, only the first difference has a large impact on the mechanism design. The second difference is purely semantic, arising from the chosen sign convention. The third has consequences on the detailed design of the system, but not on its overall function as both a load-balancing element and a transmission.

A properly designed PARITy apportions power from the single actuator in a manner that results in balanced instantaneous aerodynamic drag torques on each wing. One strategy for achieving this behavior with a drivetrain based on wing trajectory control requires three elements: a sensor to detect a drag torque imbalance, kinematic control inputs on the drivetrain to alter wing trajectories, and a control system to calculate the required wing trajectory corrections. The PARITy contains these three elements, but all are purely mechanical in nature. Torque imbalance on the wings is sensed using a mechanical "balance beam" structure. A supplemental degree of freedom allows alteration of wing trajectories. Finally, the system dynamics are tuned to behave as a control system, modulating wingstroke velocity to cancel the wing torques sensed by the balance beam. This complex dynamic behavior of the PARITy is achieved using a remarkably simple kinematic design.

3.2 Kinematics Description. The PARITy drivetrain is a symmetric 2DOF planar mechanism constructed of rigid links connected by revolute joints. A detailed diagram of the drivetrain is presented in Fig. 5. The mechanism configuration is completely specified by the two configuration variables

$$\theta_w^R(q_1,q_2) = \operatorname{atan}\left(\frac{L_4-L_2}{L_3}\right) + \operatorname{atan}\left(\frac{L_1+L_2-L_4-\frac{1}{2}L_0\sin q_2 - q_1}{L_3+\frac{1}{2}L_0(1-\cos q_2)}\right) - \operatorname{acos}\left(\frac{\left(L_3+\frac{1}{2}L_0(1-\cos q_2)\right)^2+\left(L_1+L_2-L_4-\frac{1}{2}L_0\sin q_2-q_1\right)^2+(L_4-L_2)^2+L_3^2-L_1^2}{2\sqrt{((L_4-L_2)^2+L_3^2)\left(\left(L_3+\frac{1}{2}L_0(1-\cos q_2)\right)^2+\left(L_1+L_2-L_4-\frac{1}{2}L_0\sin q_2-q_1\right)^2\right)}}\right) \quad (1)$$

q_1 and q_2. The vertical displacement of the central horizontal platform is quantified by q_1. This platform, indicated by a hatched pattern in Fig. 5, is the input of the PARITy drivetrain and will be called the *input platform*. The input platform is connected to link L_0 through a revolute joint; the rotation of link L_0 about this joint is quantified by the second configuration variable q_2. This joint will be referred to as the *fulcrum*, while the link L_0 will be called the *balance beam*.

The input platform is the attachment point for the output of the power actuator, a high energy density piezoelectric bimorph cantilever which will not be described further in this article (for details, see Ref. [14]). Power is input to the PARITy drivetrain by applying an oscillatory vertical force on the input platform, resulting in a reciprocating trajectory of q_1. The drivetrain has two outputs to drive the two wings, a "right" output and a "left" one. The right output is link L_3 (labeled in Fig. 5) on the right side of the drivetrain, while the left output is link L_3's symmetric pair on the left side of the drivetrain. The configuration of the left wing is described by a single stroke angle $\theta_w^L(q_1,q_2)$, while the configuration of the right wing is described by the angle $\theta_w^R(q_1,q_2)$. Under the constraint $q_2=0$, the resulting 1DOF system is identical to the HMF drivetrain, and oscillatory motion of q_1 produces a symmetric flapping motion of the wings characterized by $\theta_w^L=-\theta_w^R$.

The degree of freedom q_2 enables the balance beam to behave as a load-balancing element in the PARITy drivetrain, altering how power is distributed from the single power actuator to each

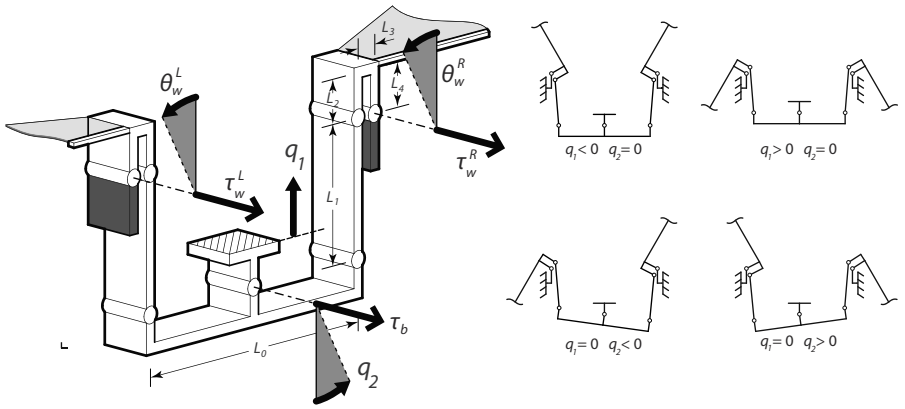

Fig. 5 PARITy drivetrain with links labeled and various angles and torques indicated. The shaded links are affixed to a mechanical ground or, in a free flying structure, an airframe. Input power is applied to the hatched input platform.

wing. Altering q_2 while holding q_1 constant results in a differential flapping motion coupling the upstroke of one wing with the downstroke of the other. This degree of freedom has no associated actuator; rather, its trajectory during operation of the PARITy drivetrain is entirely determined by the system dynamics.

As a function of the system configuration variables q_1 and q_2, exact expressions for the left and right wingstroke angles are exceedingly complex (see Eq. (1)), but are related by a simple expression

$$\theta_w^R(q_1,q_2) = -\theta_w^L(q_1,-q_2) \tag{2}$$

For design insight, a first order linearization of Eq. (1) around the neutral point results in the approximate expressions

$$\theta_w^R(q_1,q_2) \approx -\frac{1}{L_3}\left(\frac{1}{2}L_0 q_2 + q_1\right)$$

$$\theta_w^L(q_1,q_2) \approx -\frac{1}{L_3}\left(\frac{1}{2}L_0 q_2 - q_1\right) \tag{3}$$

Displacement transmission ratios relating infinitesimal balance beam rotations to changes in wing angles can be defined for the PARITy drivetrain

$$T^R(q_1,q_2) \equiv \frac{\partial \theta_w^R}{\partial q_2}(q_1,q_2)$$

$$T^L(q_1,q_2) \equiv \frac{\partial \theta_w^L}{\partial q_2}(q_1,q_2) \tag{4}$$

Combining Eq. (4) with Eqs. (1) and (2) results in closed form analytical expressions for $T^R(q_1,q_2)$ and $T^L(q_1,q_2)$, but the details of this derivation have been omitted for brevity. See Fig. 6 for a plot of $T^R(q_1,q_2)$ as a function of the wing angle $\theta_w^R(q_1,q_2)$ for the experimentally constructed PARITy drivetrain.

Displacement transmission ratios are useful for calculating wingstroke angles, but the PARITy drivetrain is one that fundamentally operates on wing *torques* as opposed to wing *angles*. An understanding of how the kinematic structure transmits torques is crucial to developing an understanding of the system dynamics. Consider a torque τ_w^R applied to the right wing (see Fig. 5). The functions $T^R(q_1,q_2)$ and $T^L(q_1,q_2)$ also serve as *torque transmission ratios*, with $T^R(q_1,q_2)$ describing how the torque τ_w^R is transmitted by the kinematic structure to appear as a torque τ_b on the balance beam L_0 about the fulcrum

$$\tau_b = T^R(q_1,q_2)\tau_w^R \tag{5}$$

At the neutral configuration $q_1=q_2=0$, the torque transmission ratios take on the following value, defined to be the constant T:

$$T^R(0,0) = T^L(0,0) = -\frac{L_0}{2L_3} \equiv T \tag{6}$$

A constant approximation $T^R(q_1,q_2) \approx T^L(q_1,q_2) \approx T$ will be used for the torque transmission ratios to simplify the theoretical analysis, though the simulation model described in Sec. 4 uses the full analytical expression, plotted in Fig. 6. For the specific incarnation of the PARITy design simulated, fabricated, and tested in this article, the dimensionless constant $T=-6.25$.

Using the constant approximation T for the torque transmission ratios and including an applied torque τ_w^L on the left wing result in the following expression for the total torque transmitted to the balance beam from both wings:

$$\tau_b = T\tau_w^L + T\tau_w^R \tag{7}$$

This torque transmission property of the PARITy transmission will be central to the discussion of its load-balancing dynamics (Sec. 3.3).

The two wings are affixed to the outputs of the PARITy drivetrain in a manner illustrated in Fig. 7. A core purpose of the wings is to produce an aerodynamic lift force to counteract gravity. Contrary to the convention for fixed wing aircraft, lift is de-

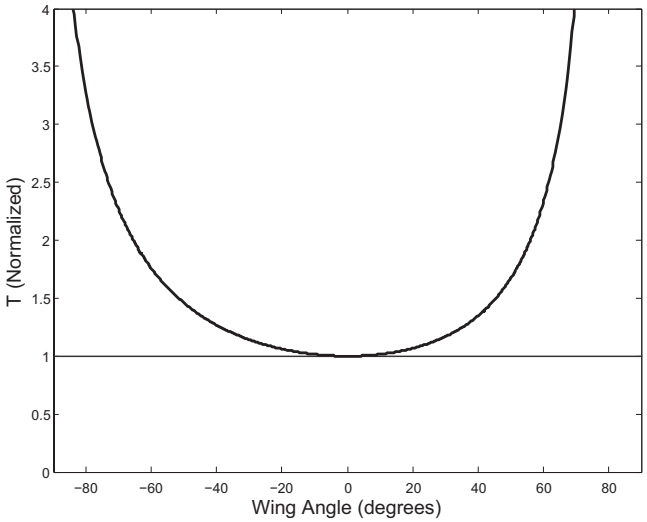

Fig. 6 The torque transmission ratio $T^R(q_1,q_2)$ (normalized to its neutral configuration value of −6.25) plotted as a function of wing angle $\theta_w^R(q_1,q_2)$ for the simulated and constructed PARITy design under the expected operating condition $q_2 \ll 1$

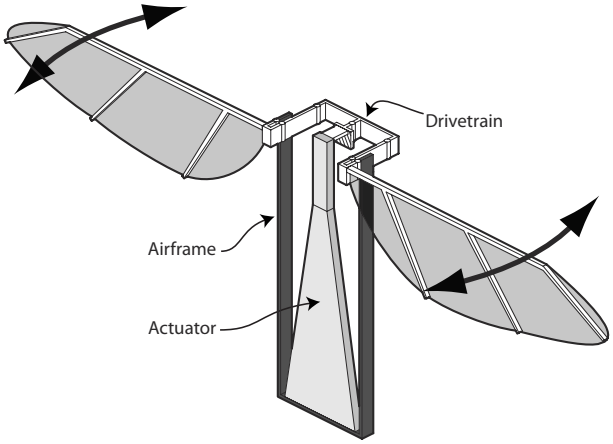

Fig. 7 Wings affixed to the PARITy drivetrain in a representative MAV. Vertical aerodynamic forces constitute lift while drag forces are perpendicular to the wing. For this experiment, wings remain perpendicular to their direction of motion, implying a fixed angle of attack α=90 deg.

fined as the component of aerodynamic forces oriented vertically in Fig. 7, similar to a rotorcraft convention. An established technique for generating lift in a flapping-wing MAV is to allow each wing to change its angle of attack α. This motion is readily observed in biological flying insects and can be actively controlled in a microrobotic insect [7,15,16]. Alternatively, passive rotation has been demonstrated to generate enough lift to support the weight of a complete aeromechanical system [8]. Though the PARITy design is expected to accommodate lift generation with actively or passively modulated angle of attack, a fixed angle of attack α=90 deg has been used to simplify the analysis of its behavior.

Given only the actuator trajectory $q_1(t)$, the wing trajectories described by $\theta_w^L(t)$ and $\theta_w^R(t)$ cannot be kinematically determined due to the passive degree of freedom q_2. An analysis of the system dynamics is necessary to determine the realized wing trajectories as well as to evaluate the performance of the PARITy drivetrain. It will be shown that under certain operating conditions, q_2 dynamically follows a trajectory that balances the aerodynamic drag torques experienced by the wings.

3.3 Simplified Dynamics Analysis

3.3.1 Automobile Torque-Balancing Dynamics. To preface an exploration of the dynamics of the PARITy drivetrain, it is useful to return to the analogy of the automobile differential. The automobile differential also introduces the additional degree of freedom q_2 (see Fig. 4) in order to balance output torques, and it is illustrative to analyze how its trajectory is determined by system dynamics. The engine shaft rotation q_1 determines the sum of wheel rotations, but the introduction of the degree of freedom q_2 removes any kinematic constraint on the difference of wheel rotations. To determine the trajectory of q_2 for a car in normal driving conditions, it is sufficient to assume that the wheels have enough grip on the driving surface so that an abnormally large torque is required to cause a wheel to slip against the ground. Delivering a balanced torque to each wheel prevents a single wheel from receiving an abnormally large torque, and so in effect enforces a "no-slip" condition on the drive wheels. This condition constrains the wheels to rotate with fixed relative angular velocities dependent on the system configuration (e.g., the steering wheel angle), a constraint that fully determines q_2 given an actuation input q_1. Thus, in normal conditions, q_2 follows a trajectory that allows the wheels to satisfy the no-slip condition.

The dynamics of the PARITy are decidedly more complex because there is no no-slip condition on the end-effectors of a flapping-wing MAV. In the absence of the no-slip condition, q_2 follows a more complex trajectory determined by the specific dynamics of the system. The automotive analogy will not provide further insight, so what follows is a simplified dynamics analysis specific to the PARITy drivetrain in the context of flapping-wing flight.

3.3.2 Torques From Flapping Wings. In the following discussion, it will be assumed that an actuation force is applied such that $q_1(t)$ undertakes a sinusoidal trajectory in time. This assumption reduces the system to one in which q_2, the rotation of the balance beam about the fulcrum, is the single degree of freedom. This simplification is illustrative in that it isolates the load-balancing differential component in the PARITy design.

The flapping motion of the wings will cause them to exert torques τ_w^L and τ_w^R at the outputs of the PARITy drivetrain. These wing torques arise from two distinct sources:

1. $\tau_{w,\text{inertial}}$—the Newtonian reaction torque resisting wing acceleration
2. $\tau_{w,\text{drag}}$—the torque resulting from the aerodynamic drag forces exerted by the ambient fluid on the wing

The total torques exerted by the wings on the drivetrain outputs can be represented as the sum of contributions from the following two sources:

$$\tau_w^L = \tau_{w,\text{drag}}^L + \tau_{w,\text{inertial}}^L$$

$$\tau_w^R = \tau_{w,\text{drag}}^R + \tau_{w,\text{inertial}}^R \tag{8}$$

The inertial reaction torque of a wing is straightforward to quantify. The following is an expression for the inertial torque due to the right wing:

$$\tau_{w,\text{inertial}}^R = -I^R \ddot{\theta}_w^R \tag{9}$$

In the preceding equation, the quantity I^R is the total moment of inertia of the right wing about its wing pivot.

Aerodynamic drag torques result from a variety of fluid effects, some of which depend on not only the instantaneous state of the system, but also on its time history. Modeling the aerodynamic drag torque is a rich research question in and of itself, but for this analysis a simplified expression produced by a blade-element model will be used.

First, define the *drag parameter* of the right wing (Ω^R) as follows:

$$\Omega^R \equiv \tfrac{1}{2}\rho \int r^3 c^R(r)\mathrm{d}r \tag{10}$$

In the preceding expression, ρ is the fluid density, $c^R(r)$ is the chordwise dimension of the right wing at a distance r from the wing pivot, and the limits of the integral are chosen to cover the entire wing extent. The aerodynamic behavior of the left and right wings is captured by their associated drag parameters Ω^R and Ω^L (see Table 1 for experimental values). The blade-element model produces the following expression for the drag torque applied by the right wing, assuming no external fluid flow (see Ref. [17]):

$$\tau_{w,\text{drag}}^R = -\Omega^R C_D(\alpha)\,\text{sgn}\ \dot{\theta}_w^R(\dot{\theta}_w^R)^2 \tag{11}$$

The quantity C_D is the characteristic drag coefficient of the wing and is a function of the angle of attack α. The drag coefficient is estimated according to the following relationship between the drag coefficient and angle of attack, derived experimentally from force measurements on dynamically scaled wings flapping in mineral oil [18]:

$$C_D(\alpha) = 1.92 - 1.55\cos(2.04\alpha - 9.82\ \text{deg}) \tag{12}$$

The fixed angle of attack α=90 deg representative of this analysis (see Fig. 7) results in a drag coefficient C_D=3.46.

Table 1 Simulation results comparing the displacement-balancing HMF drivetrain with the torque-balancing PARITy drivetrain

Drivetrain	Trial	Ω^R (mg mm^2)	Ω^L (mg mm^2)	$\Delta\tau_{w,\mathrm{drag}}$ [a] (mN mm)	$\tau^R_{w,\mathrm{drag}}$ [a] (mN mm)	$\tau^L_{w,\mathrm{drag}}$ [a] (mN mm)	Drag torque imbalance (%)	
							Instantaneous	Peak
HMF	Control	31.3	31.3	0.00	12.42	12.42	0.0	0.0
	1-cut	31.3	18.8	5.52	13.78	8.26	40.1	40.1
	2-cut	31.3	13.2	8.32	14.35	6.03	58.0	58.0
PARITy	Control	31.3	31.3	0.03	12.46	12.47	0.2	0.1
	1-cut	31.3	18.8	0.97	10.73	10.77	9.0	0.3
	2-cut	31.3	13.2	1.46	9.56	9.46	15.3	1.0

[a]Peak magnitude over wingstroke.

3.3.3 Mechanical Torque Feedback. The torques τ^L_w and τ^R_w, calculated from Eqs. (9) and (11), act on the balance beam L_0 about the fulcrum due to the kinematic torque transmission mechanism. Since the mass of the balance beam itself is negligible, this torque τ_b must effectively be zero, so from Eq. (7), the following relationship must hold:

$$\tau^L_w = -\tau^R_w \tag{13}$$

This equation represents the equilibrium condition of the PARITy drivetrain and is fundamental to its operation. Simply put, a system operating at this equilibrium point will deliver torques of equal magnitude to each wing about its respective wing pivot. Recall, however, that these wing torques arise from both inertial and aerodynamic sources. If the inertial torques are small compared with the aerodynamic drag torques, then a PARITy drivetrain operating in this equilibrium will flap the wings in a manner that balances the aerodynamic drag torques experienced by the wings.

Inertial torques are largest at the extremes of the wingstroke where the angular wing acceleration is maximal. Ignoring complex and unmodeled effects at stroke reversal, drag torques tend to be largest when the wing is midstroke near its maximum angular velocity. This phase dependence of the inertial and drag torques is apparent in Fig. 8.

Should inertial torques dominate, from Eq. (9) it can be shown that the balance beam experiences a restoring torque if $\ddot{\theta}^L_w$ and $\ddot{\theta}^R_w$ are perturbed from equilibrium, implying a feedback loop sensitive to errors in $\ddot{q}_2$. Should aerodynamic torques dominate, the aerodynamic model used in this study also results in a negative feedback loop; however, the aerodynamically dominated system responds to wing velocity as opposed to acceleration, and is sensitive to errors in $\dot{q}_2$. The situation is more complex when inertial torques are of comparable magnitude to aerodynamic torques, but resorting to the full dynamics simulation (Sec. 4) results in no apparent stability problems.

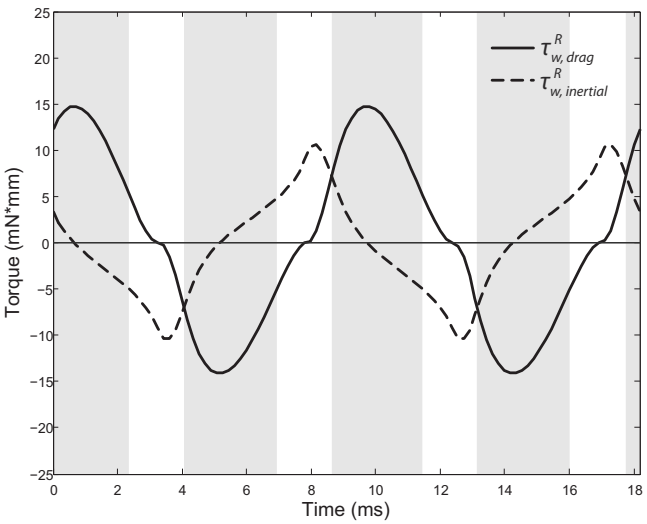

Fig. 8 Theoretical torques $\tau^R_{w,\mathrm{drag}}$ and $\tau^R_{w,\mathrm{inertial}}$ applied by the right wing in a symmetric system. In shaded regions, $|\tau^R_{w,\mathrm{drag}}| > |\tau^R_{w,\mathrm{inertial}}|$.

It is to be noted that the drag torque feedback loop is sensitive to $\dot{q}_2$ and the inertial torque feedback loop is sensitive to $\ddot{q}_2$, but neither is sensitive to the balance beam angle q_2. Though these two feedback loops are dominant on a subwingstroke timescale, neither will correct for a gradual drift of q_2 occurring over a timescale encompassing many wingstrokes. Such a drift would affect the midpoint angles of each wingstroke, which, if allowed to drift over a large range, may adversely affect the performance of the system.

To address this issue, it is necessary to revisit Eq. (7). This equation for the torque τ_b on the balance beam has neglected an internal torque contribution. In a physical incarnation of the PARITy drivetrain (see Sec. 5), revolute joints are achieved using polymer flexures, which act as torsion springs [4]. This spring torque τ_k always acts to restore the balance beam to horizontal ($q_2 \rightarrow 0$), but the magnitude of this torque can be made to be negligible compared with the typical magnitudes of $T\tau^L_w$ and $T\tau^R_w$ for subwingstroke dynamics. Augmenting Eq. (7) to incorporate the spring torque results in the following expression for the torque on the balance beam:

$$\tau_b = T\tau^L_w + T\tau^R_w + \tau_k \tag{14}$$

Though τ_k is negligible on the subwingstroke timescale, it is the only torque that responds to a slowly drifting value of q_2. If the trajectory of q_2 is offset from zero, τ_k biases the system in a way that tends to correct it. An important design consideration is to set the torsional spring constants such that τ_k provides ample resistance to a drifting balance beam angle without substantially impacting wingstroke dynamics.

For simplicity, this discussion of the PARITy drivetrain dynamics has used a linear approximation of mechanism kinematics. It is important to confirm, however, that the full nonlinear system indeed exhibits the torque-balancing characteristics implied by this linearized analysis. To provide this confirmation, a numerical simulation of the full nonlinear system dynamics was developed.

4 Dynamics Simulation

4.1 Simulation Characteristics. A pseudorigid body model is an excellent approximation for an insect-scale PARITy drivetrain realizable with the smart composite microstructure (SCM) fabrication techniques [4,19]. Using this model, links are assumed to be infinitely stiff while the joints are modeled as perfect revo-

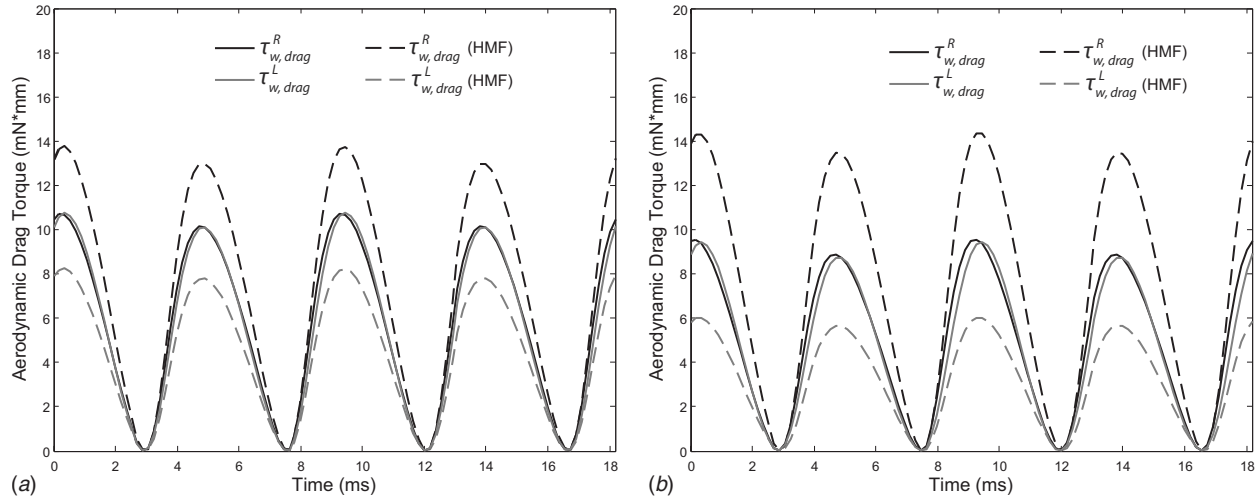

Fig. 9 Simulated drag torque magnitudes. For both results, the right wing has a torque parameter Ω^R=31.3 mg mm^2. The left wing drag parameter Ω^L has been reduced to (*a*) 0.599·Ω^R and (*b*) 0.420·Ω^R.

lute joints in parallel with torsion springs. The associated spring constants are derived from standard beam theory (see Ref. [4] for details).

The piezoelectric bimorph actuator is modeled as a linear spring in parallel with a time-varying force. Both the spring constant and the force amplitude were calculated from known dimensions and material properties using a laminate plate theory model [14].

The only modeled inertias are those of the two wings, dominating the negligible and unmodeled mass of the PARITy drivetrain mechanism itself. Though actuator mass is nominally large, due to the large transmission ratio coupling actuation stroke to wingstroke, the effective actuator mass is negligible and its impact has not been modeled.

Aerodynamic drag torque on the wing is modeled according to Eq. (11). The full nonlinear torque transmission ratios $T^R(q_1,q_2)$ and $T^L(q_1,q_2)$ are incorporated into the simulation code.

The two configuration variables q_1 and q_2 along with their time derivatives $\dot{q}_1$ and $\dot{q}_2$ completely specify the state of the system. An Euler–Lagrange formulation produces a set of two coupled second order nonlinear differential equations for $q_1(t)$ and $q_2(t)$. The aerodynamic drag torques on each wing enter the simulation model as generalized forces, while a third generalized force is the time-varying force exerted by the actuator.

These differential equations have been integrated numerically in MATLAB using the Runge–Kutta based routine ode45. In all simulations described in this article, the actuator force is varied sinusoidally in time with zero mean, a peak-to-peak amplitude of 242.5 mN (predicted from a 200 V drive signal; see Ref. [14]), and a frequency of 110 Hz. The drive frequency is tuned to the observed mechanical resonance of the realized experimental structure (Sec. 5).

4.2 Performance. The primary benefit of the PARITy drivetrain is its ability to passively compensate for asymmetric aerodynamic conditions. These can arise from factors external to the microrobotic insect, such as wind gusts or thermal variations, or they can arise from internal factors such as asymmetries due to fabrication variation or degradation during operation. Asymmetry of the wing membranes, accurately achievable in a laboratory setting, was used to assess the performance of the PARITy in comparison to the baseline HMF drivetrain, which exhibits no load-balancing characteristics. A "control" simulation of the two drivetrains was conducted with symmetric wing parameters. Since $\Omega^L_{\text{Control}}=\Omega^R$, both the HMF and the PARITy drivetrains produce balanced aerodynamic drag torques on each wing in the control trial.

Removing a section of the wing membrane effectively reduces the area of the wing planform. If the left wing is altered in this manner, its drag parameter Ω^L will be smaller than Ω^R of the unaltered right wing. The HMF drivetrain will always produce symmetric trajectories for the wings, meaning that their angular velocities are constrained to be equal and opposite. If membrane removal from the left wing results in its drag parameter being 59.9% of the drag parameter of the right wing, we expect from Eq. (11) that the use of the HMF drivetrain will result in the drag torque experienced by the left wing to be 59.9% of that experienced by the right wing at every point in time. The condition $\Omega^L_{\text{1-cut}}=0.599\cdot\Omega^R$ will be called the "1-cut" trial, and the drag torques experienced by each wing using the HMF drivetrain are illustrated in Fig. 9(*a*). The results of a second trial, the "2-cut" trial, in which the left wing's torque parameter has been reduced to 42.0% of that of the right wing ($\Omega^L_{\text{2-cut}}=0.420\cdot\Omega^R$) are shown in Fig. 9(*b*). The system parameters for these two trials are chosen to correspond with that realized by the experimental procedure (Sec. 5).

In contrast with the HMF drivetrain, the PARITy drivetrain does not constrain the wingstroke angles to have symmetric trajectories. The load-balancing characteristics of the transmission act to match the aerodynamic drag torques even in the presence of drastically asymmetric drag parameters. Figure 9 illustrates that with the use of the PARITy drivetrain, the aerodynamic drag torques experienced by both the left and right wings have been passively balanced by the system dynamics.

To quantitatively evaluate the simulated performance of the PARITy drivetrain relative to the baseline HMF drivetrain, the metrics have been defined, relevant once periodic operation has been established. The first is the *peak* drag torque imbalance, defined as the difference between the maximum drag torque magnitudes experienced by each wing over 1 cycle. The second is the *instantaneous* drag torque imbalance, defined to be the maximum value of the torque discrepancy $\Delta\tau_{w,\text{drag}}$ over 1 cycle. Both metrics are normalized to the maximum drag torque experienced by the right wing over 1 cycle. The drag torque discrepancy $\Delta\tau_{w,\text{drag}}$ is defined as

$$\Delta\tau_{w,\text{drag}} \equiv \tau^L_{w,\text{drag}} + \tau^R_{w,\text{drag}} \tag{15}$$

Note that when the drag torques on the wings are balanced, $\Delta\tau_{w,\text{drag}}=0$. Table 1 summarizes the performance of the HMF and PARITy drivetrains in the control, 1-cut, and 2-cut trials.

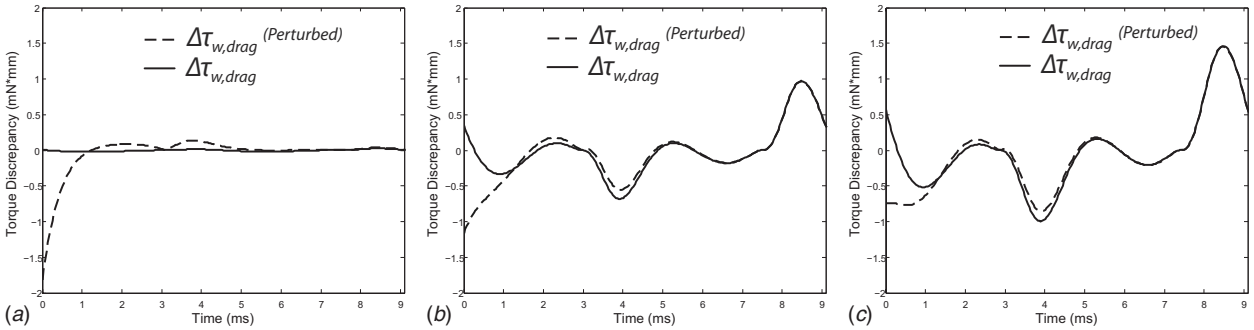

Fig. 10 Solid lines indicate the instantaneous torque discrepancy $\Delta\tau_{w,\text{drag}}$ between wings over a single cycle when (*a*) $\Omega^L_{\text{control}}=\Omega^R$, (*b*) $\Omega^L_{\text{1-cut}}=0.599\cdot\Omega^R$, and (*c*) $\Omega^L_{\text{2-cut}}=0.420\cdot\Omega^R$. The dashed lines describe the recovery of the torque imbalance from a 2 rad/s perturbation applied to the balance beam rotational velocity $\dot{q}_2$ at time $t=0$.

The peak drag torque imbalance metric compares the amplitudes of the drag torques while ignoring their phase relationship. In the 1-cut trial, the HMF drivetrain exhibits a peak drag torque imbalance of 40.1%, expected due to $\Omega^L_{\text{1-cut}}=0.599\cdot\Omega^R$. The use of the PARITy, however, reduces this peak drag torque imbalance to 0.3%. In the 2-cut trial, the peak torque imbalance of 58% exhibited by the HMF drivetrain is reduced to 1.0% with the use of the PARITy drivetrain. Performing remarkably well, the PARITy drivetrain reduces the peak drag torque imbalance by a factor of 133 in the 1-cut trial and a factor of 58 in the 2-cut trial.

The instantaneous drag torque imbalance metric reports the maximum drag torque discrepancy $\Delta\tau_{w,\text{drag}}$ experienced during a wingstroke, relative to the peak drag torque magnitude of the unaltered wing. For the 1-cut trial, an instantaneous drag torque imbalance of 40.1% exhibited by the HMF drivetrain is reduced to 9.0% by the PARITy drivetrain. For the 2-cut trial, the HMF drivetrain's instantaneous drag torque imbalance of 58% is reduced to 15.3% by the PARITy drivetrain. Though the PARITy drivetrain still performs well, a slight phase shift between the drag torques on each wing impacts its performance under the instantaneous drag torque metric. The drag torque discrepancy $\Delta\tau_{w,\text{drag}}$ is plotted over a single wingstroke in Fig. 10.

In order to investigate the damping properties and time response of the torque-balancing feedback loops, a perturbation was applied to the system in the form of a step change in $\dot{q}_2$ of 2 rad/s. This perturbation roughly corresponds to a 0.36 mN mm ms angular impulse applied to both wings. The impulse upsets the normal operation of the PARITy drivetrain, and the dashed lines in Fig. 10 illustrate the recovery of $\Delta\tau_{w,\text{drag}}$. The drivetrain returns smoothly to periodic operation, regaining much of its steady state character with a time constant on the order of 1 ms. For all trials, the perturbed performance is indistinguishable from that of the unperturbed system in less than one wingstroke (9.1 ms).

4.3 Unmodeled Effects. Many aerodynamic models predict that airfoils experience aerodynamic forces proportional to accelerations, an effect often handled by adding extra mass to the mass of the airfoil. This "virtual mass" term is difficult to calculate, but theoretical expressions exist to estimate the virtual mass of simple wing planforms [1]. However, these expressions are not applicable to complex planforms, and the correction to the airfoil mass must be either measured experimentally or neglected.

This is especially true for investigating the performance of wings after membrane removal, where even the "flat plate" model of the wing is likely to fail. In this case, not only are theoretical virtual mass calculations difficult, but also the accuracy of the blade-element model is degraded. In this study, the virtual mass has been neglected and, for lack of a better aerodynamic model, the drag parameters have been estimated by use of the blade-element model. The poor estimation of the drag parameters of complex wing planforms is a source of error for experimental verification of the theoretical model.

A final effect that has not been modeled is the measurable amount of elastic deformation experienced by the leading wing spar at typical aerodynamic and inertial loads. However, this effect is expected to have a negligible impact on the system behavior.

5 Experimental Verification

5.1 Methods. In order to experimentally verify the theoretical performance of the PARITy drivetrain design, an at-scale PARITy has been fabricated using SCM fabrication techniques [4]. The drivetrain is a symmetric structure consisting of links of the following lengths:

L_0	L_1	L_2	L_3	L_4
5000 μm	2500 μm	800 μm	400 μm	800 μm

These values produce a PARITy drivetrain that maps a ± 200 μm actuation stroke into an approximately ± 35 deg wingstroke (see Fig. 13). This is smaller than the wingstroke amplitude used to demonstrate a lift force greater than aeromechanical system mass [8]. However, reducing wing membrane area is expected to increase wing amplitude, and a conservative baseline stroke amplitude is required to accommodate the extreme removal of wing membrane tested in the 2-cut trial.

The transmission and actuator were mounted into a high-stiffness test structure (Fig. 11) forming a nearly ideal mechanical ground. Two wings identical to within manufacturing tolerances were fabricated using structural carbon fiber spars and a 1.5 μm thick polyester wing membrane. As fabricated, these wings, shown in Fig. 12, have a mass of 834 μg and a moment of inertia around the wing pivot equal to 29.0 mg mm^2. The wings extend 16.0 mm beyond the wing pivot, with an effective planform area of 51.4 mm^2 (Fig. 12(*a*)). Using Eq. (11), the drag parameters Ω^R and $\Omega^L_{\text{Control}}$ were both calculated to be 31.3 mg mm^2 for the control trial.

A 110 Hz sinusoidal drive signal with a constant 200 V peak-to-peak amplitude was applied to the piezoelectric bimorph actuator. Wing trajectories were recorded using a high-speed video camera operating at 10,000 frames per second, approximately 91 frames per wingstroke (see Fig. 15). Wing angles were extracted from the video stream with image analysis software, producing about 91 data points per wingstroke over 10 wingstrokes for the control trial.

For the 1-cut trial, the data collection process was repeated after removing a section of the left wing membrane, reducing the wing planform area to 84.3% of its area in the control trial. The drag

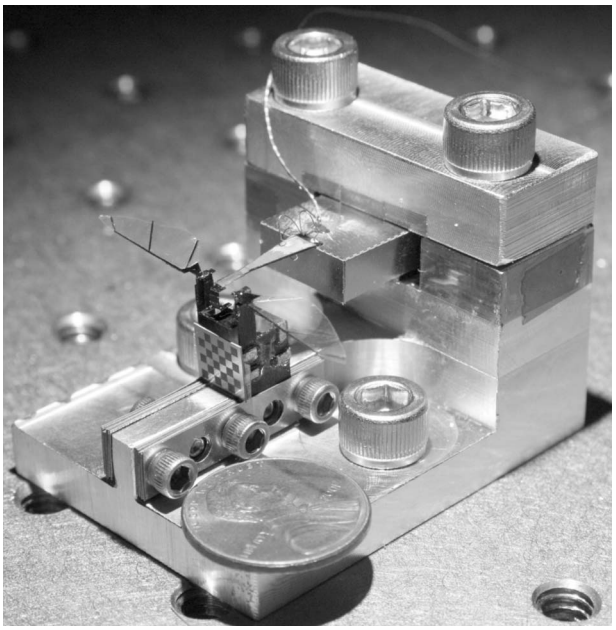

Fig. 11 The experimental test structure

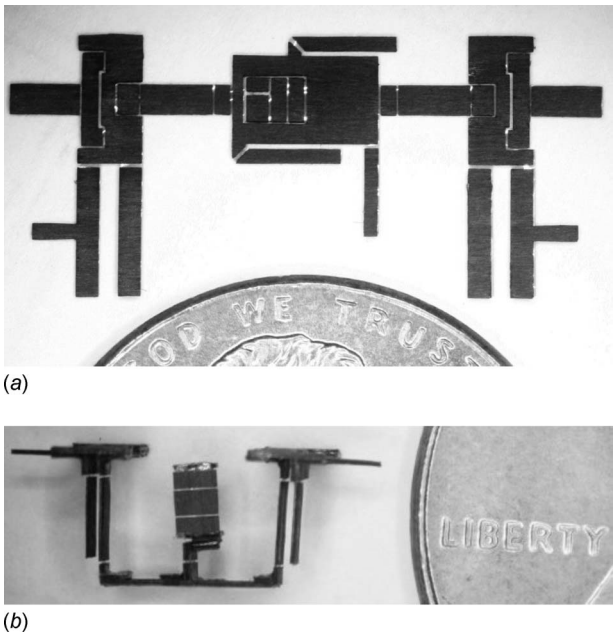

Fig. 13 The PARITy drivetrain (*a*) before and (*b*) after folding

parameter was recalculated using Eq. (11), resulting in a modified drag parameter $\Omega^L_{1\text{-cut}}=18.8$ mg mm^2, or 59.9% of Ω^R. The moment of inertia I^L of the left wing is not appreciably changed by the removal of wing membrane mass. For the 2-cut trial, an additional section of wing membrane was removed, leaving 56.8% of the original wing planform resulting in $\Omega^L_{2\text{-cut}}=13.2$ mg mm^2, or 42.0% of Ω^R. Again, I^L remains effectively constant due to the negligible contribution of the wing membrane mass to the moment of inertia. The wing planforms for all three trials are displayed in Fig. 12.

Elastic deformation of the wings resulted in a discrepancy of as much as 8 deg between the angle of the distal end of the leading wing spar and the angle of the proximal end at the output of the PARITy drivetrain. In order to minimize the impact of this elastic deformation, wingstroke angles were extracted by tracking points on the leading wing spar extending no more than 5 mm from the drivetrain output.

5.2 Results and Discussion. The experimental wing trajectories for the control, 1-cut, and 2-cut trials are plotted in Figs. 14(*a*)–14(*c*), along with the trajectories predicted by simulation. It is important to note that the phase relationship between the drive signal itself and the wing trajectory data from the video stream was not experimentally recorded. The theoretical predictions were aligned in time with experimental data by matching the phase of the fundamental 110 Hz components of predicted and experimental $\theta^R_w(t)$. This technique does not allow verification of the predicted phase shift between drive signal and wing trajectory, but it allows verification of the relative phase shift between the trajectories of the left and right wings.

In the control trial, the symmetry of the system demands symmetric wing trajectories. However, fabrication tolerances have created measurable errors. Two such effects are readily apparent in the experimental data.

1. The mean right wingstroke angle is −9.5 deg while the mean left wingstroke angle has a magnitude of less than 0.5 deg (both removed from Fig. 14).

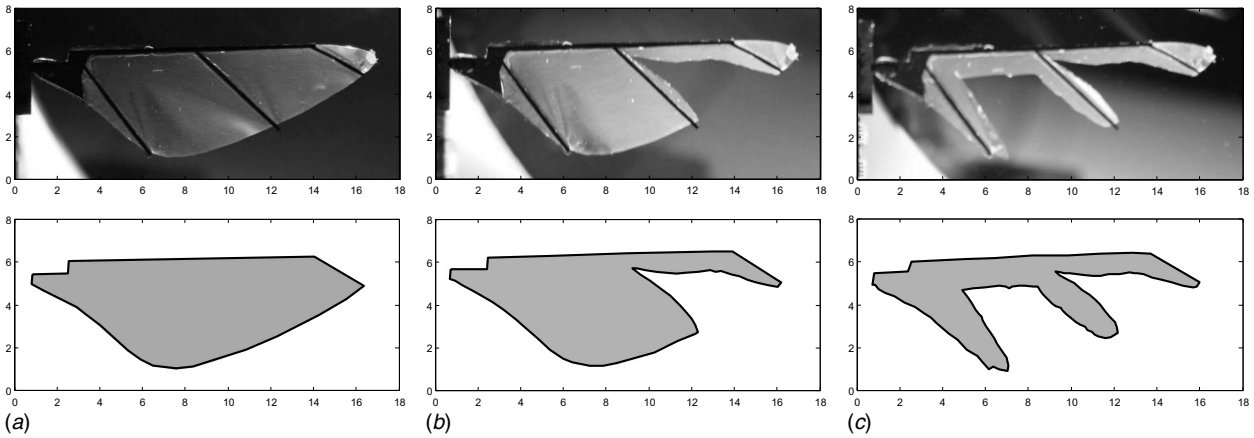

Fig. 12 Images of the left wing membrane as used for each trial, along with the associated planforms used to calculate the drag parameter Ω^L using the blade-element model. Units are in millimeters. (*a*) Control trial, $\Omega^L_{\text{control}}=31.3$ mg mm^2. (*b*) 1-cut trial, $\Omega^L_{\text{1-cut}}=18.8$ mg mm^2. (*c*) 2-cut trial, $\Omega^L_{\text{2-cut}}=13.2$ mg mm^2.

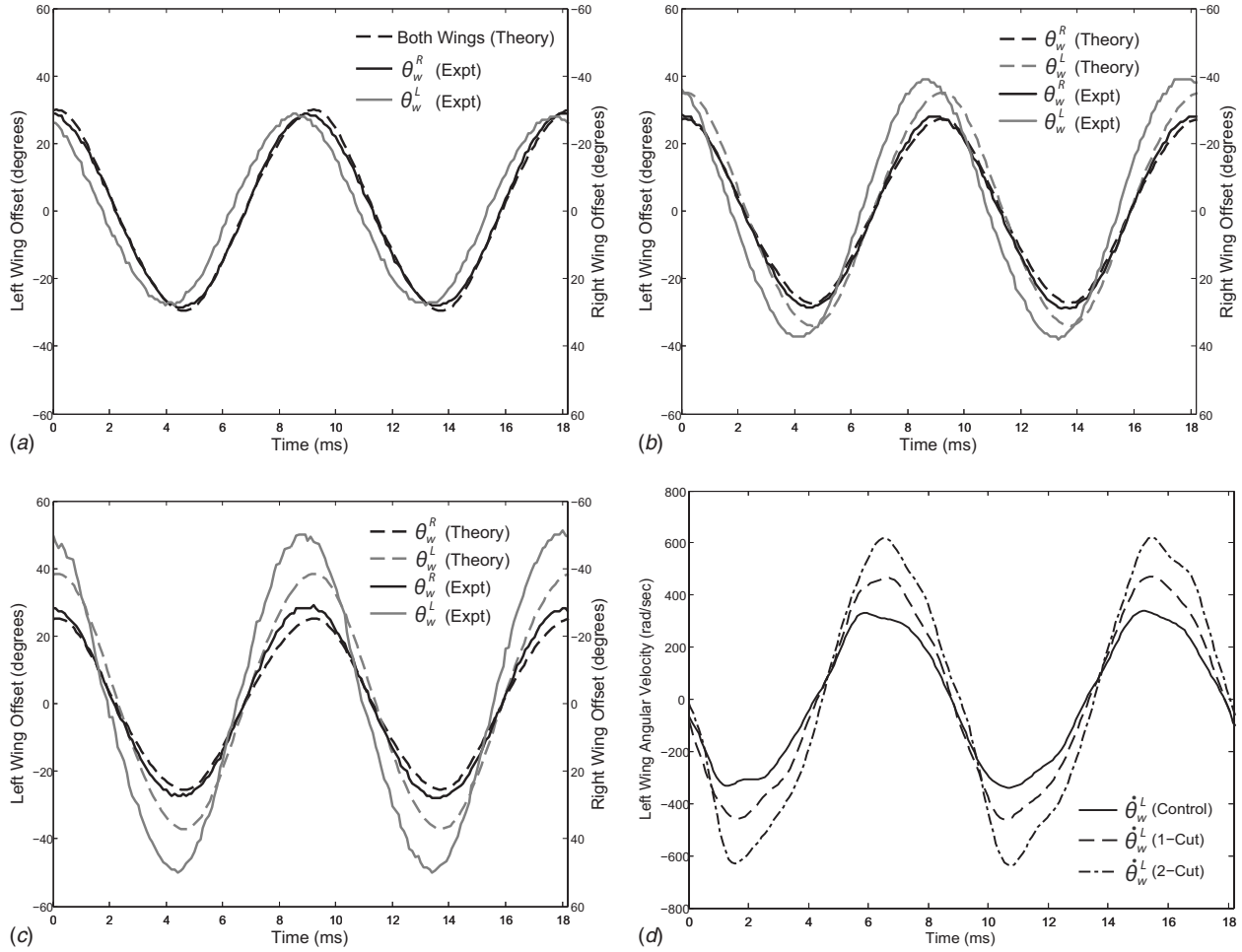

Fig. 14 Theoretical predictions versus experimental wing trajectories for (*a*) the control trial, (*b*) the 1-cut trial, and (*c*) the 2-cut trial. (*d*) Experimentally observed left wing velocities, low-pass filtered with an 800 Hz cutoff frequency.

2. The fundamental 110 Hz oscillation of $\theta_w^L(t)$ leads that of $\theta_w^R(t)$ by 0.45 ms, a phase difference equal to 5.0% of a full flapping cycle.

Simulation of the control trial produces mean stroke angles of less than 0.5 deg in magnitude. The observed mean right wing-stroke angle of −9.5 deg in the experimental trial can be attributed to an offset in the minimum potential energy configuration of the experimental test structure, likely caused by fabrication error. The exact cause of this offset could not be isolated, and it has been removed from plots of experimental data.

The removal of the mean stroke angle is expected to have only a minor impact on the predicted wing trajectory because, when the wing is less than 40 deg from horizontal, the transmission ratio is relatively insensitive to wing angle (Fig. 6). However, the 2-cut experimental trial has a stroke amplitude approaching ±50 deg, so the nonzero mean stroke angle may contribute to the discrepancy between theory and experiment in this trial.

The phase difference of wing trajectories in the control trial can be seen in Fig. 14(*a*). A symmetric system should not exhibit any phase difference but there are many possible asymmetries that can

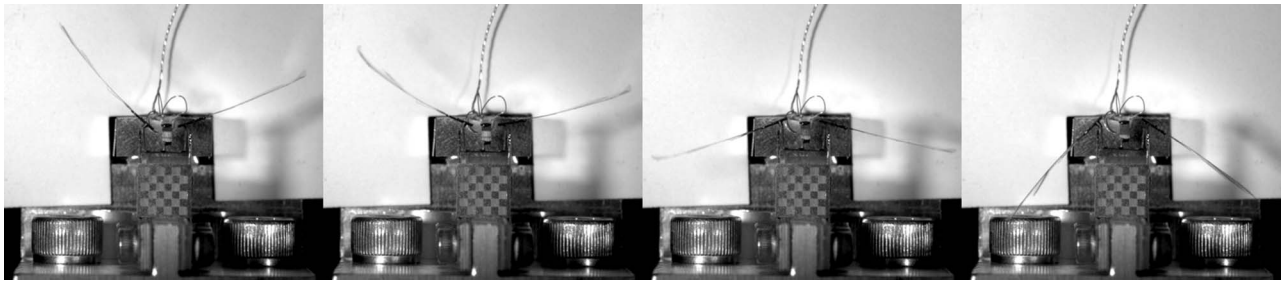

Fig. 15 Image sequence from the 2-cut trial high speed video illustrating increased amplitude of θ_w^L compared with θ_w^R. From left to right, the elapsed time between adjacent images is 1.5 ms. The checkerboard contains 1×1 mm² squares and is used for scale.

cause it. A difference between torsion spring constants in the transmission can lead to phase errors, as can mismatched wing inertias or transmission ratios caused by fabrication variation.

However, these asymmetries aside, Figs. 14(*b*) and 14(*c*) provide clear evidence that the PARITy drivetrain manages the distribution of actuator power to compensate for asymmetric loading torques. The stroke amplitude of the left wing is increased in the 1-cut trial to compensate for its reduced membrane area. It is larger still in the 2-cut trial, where even more membrane area has been removed. The predicted wing trajectories demonstrate close, if not perfect, agreement with the experimental data. The increase in wing velocity as membrane is removed can be seen more clearly in Fig. 14(*d*).

The experimental wing trajectories correspond well with theoretical predictions of the simulation model. The theoretical model slightly underestimates the stroke amplitude increase in the altered wing in both the 1-cut and 2-cut trials, an effect which can be attributed to overestimation of the drag parameters assigned to the complex altered wing planforms used in these trials. Though the drag torques were not directly measured in this test setup, the increased stroke amplitude of the wing with a reduced planform area is indirect evidence of the drag torque-balancing nature of the PARITy drivetrain. Using a passive mechanism, the PARITy distributes power from the actuator in a manner that compensates for the altered wing's reduced capacity to induce aerodynamic drag torques.

6 Conclusion

The PARITy is a first incarnation of a MAV drivetrain that includes mechanical features designed to passively balance aerodynamic forces created by two flapping wings. Experimental and theoretical results have shown that a PARITy drivetrain scaled to operate on a platform of a similar scale to Dipteran insects succeeds in passively balancing aerodynamic drag torques. The PARITy's tuned dynamic behavior has been realized with negligible increases in kinematic complexity and system mass as compared with the baseline HMF design.

Future generations of the PARITy drivetrain will advance the design paradigm of using mechanical feedback mechanisms and tuned system dynamics to allow deterministic control of aerodynamic force relationships between the two wings. Immediate research goals toward this end fall into three categories:

1. demonstrating compatibility of PARITy designs with lift generating features
2. including passive mechanisms sensitive to lift forces in conjunction with drag forces
3. incorporating active inputs to alter drivetrain dynamics during operation, providing control over aerodynamic force relationships between the wings

Many components of the PARITy drivetrain are inherited from the HMF, a biomimetic system fundamentally inspired by Dipteran insects. However, there is little research exploring whether passive mechanical structures similar to the PARITy's balance beam play an important role in airborne biological organisms. It is interesting to note that during the 2-cut trial, in which almost half of the left wing planform area was removed, the PARITy's passive mechanisms resulted in a 53% increase in the angular amplitude of the left wing compared with that of the right one. This drastic increase in wing amplitude was achieved with the balance beam undergoing passive oscillatory rotation with peak-to-peak amplitude of only 1.7 deg. This result suggests that even a small amount of mechanical compliance in a flapping-wing drivetrain can give rise to significant passive feedback mechanisms operating on aerodynamic forces. Accordingly, this work suggests an investigation into whether passive mechanisms similar to the PARITy balance beam play an important role in the drivetrains of flight-capable biological insects.

Acknowledgment

The authors gratefully acknowledge support from the National Science Foundation (Award No. CMMI-07466 38). Any opinions, findings and conclusions or recommendations expressed in this material are those of the authors and do not necessarily reflect those of the National Science Foundation.

References

[1] Dudley, R., 2000, *The Biomechanics of Insect Flight: Form, Function, Evolution*, Princeton University Press, Princeton, NJ.
[2] Dickinson, M. H., and Tu, M. S., 1997, "The Function of Dipteran Flight Muscle," Comp. Biochem. Physiol. Part A: Physiology, **116**(3), pp. 223–238.
[3] Sunada, S., and Ellington, C. P., 2001, "A New Method for Explaining the Generation of Aerodynamic Forces in Flapping Flight," Math. Methods Appl. Sci., **24**, pp. 1377–1386.
[4] Wood, R. J., Avadhanula, S., Sahai, R., Steltz, E., and Fearing, R. S., 2008, "Microrobot Design Using Fiber Reinforced Composites," ASME J. Mech. Des., **130**, p. 052304.
[5] Hoover, A. M., Steltz, E., and Fearing, R. S., 2008, "RoACH: An Autonomous 2.4 g Crawling Hexapod Robot," IEEE/RSJ International Conference on Intelligent and Robots and Systems, pp. 26–33.
[6] Baisch, A. T., and Wood, R. J., 2009, "Design and Fabrication of the Harvard Ambulatory Microrobot," 14th International Symposium on Robotics Research.
[7] Yan, J., Avadhanula, S. A., Birch, J., Dickinson, M. H., Sitti, M., Su, T., and Fearing, R. S., 2001, "Wing Transmission for a Micromechanical Flying Insect," J. Micromechatronics, **1**(3), pp. 221–237.
[8] Wood, R. J., 2008, "The First Takeoff of a Biologically Inspired At-Scale Robotic Insect," IEEE Trans. Robot., **24**, pp. 341–347.
[9] Finio, B., Shang, J., and Wood, R. J., 2009, "Body Torque Modulation for a Microrobotic Fly," IEEE International Conference on Robotics and Automation.
[10] Tu, M. S., and Dickinson, M. H., 1996, "The Control of Wing Kinematics by Two Steering Muscles of the Blowfly (Calliphora Vicina)," J. Comp. Physiol., A, **178**(6), pp. 813–830.
[11] Tanaka, H., Hoshino, K., Matsumoto, K., and Shimoyama, I., 2005, "Flight Dynamics of a Butterfly-Type Ornithopter," 2005 IEEE/RSJ International Conference on Intelligent and Robots and Systems, pp. 2706–2711.
[12] Pornsin-Sirirak, T. N., Tai, Y. C., Ho, C. M., and Keennon, M., 2001, "Microbat: A Palm-Sized Electrically Powered Ornithopter," Proceedings of NASA/JPL Workshop Biomorphic Robotics, pp. 14–17.
[13] Madangopal, R., Khan, Z. A., and Agrawal, S. K., 2005, "Biologically Inspired Design of Small Flapping Wing Air Vehicles Using Four-Bar Mechanisms and Quasi-Steady Aerodynamics," ASME J. Mech. Des., **127**, pp. 809–816.
[14] Wood, R. J., Steltz, E., and Fearing, R. S., 2005, "Optimal Energy Density Piezoelectric Bending Actuators," Sens. Actuators, A, **119**(2), pp. 476–488.
[15] Fry, S. N., Sayaman, R., and Dickinson, M. H., 2005, "The Aerodynamics of Hovering Flight in Drosophila," J. Exp. Biol., **208**(12), pp. 2303–2318.
[16] Fry, S. N., Sayaman, R., and Dickinson, M. H., 2003, "The Aerodynamics of Free-Flight Maneuvers in Drosophila," Science, **300**, pp. 495–498.
[17] Ellington, C. P., 1984, "The Aerodynamics of Hovering Insect Flight. IV. Aerodynamic Mechanisms," Philos. Trans. R. Soc. London, Ser. B, **305**, pp. 79–113.
[18] Dickinson, M. H., Lehmann, F. O., and Sane, S. P., 1999, "Wing Rotation and the Aerodynamic Basis of Insect Flight," Science, **284**, pp. 1954–1960.
[19] Howell, L. L., 2001, *Compliant Mechanisms*, Wiley, New York.